

Article

A Sustainable Amine Magnetic Biocomposite Based on Rice Husk–Sugarcane Bagasse Fiber for Lead and Contaminant Adsorption in Aqueous Solution

Iryanti Fatyasari Nata^{1,2,*}, Chairul Irawan¹, Meilana Dharma Putra¹, Hesti Wijayanti¹, Yuniza Shentya Dewi¹ and Yenny Meliana³

¹ Department of Chemical Engineering, Lambung Mangkurat University, Banjarbaru 70714, Indonesia

² Wetland-Based Materials Research Centre, Institution of Research and Community Services, Lambung Mangkurat University, Banjarbaru 70714, Indonesia

³ The National Research and Innovation of Indonesia, Tangerang 15314, Indonesia

* Correspondence: ifnata@ulm.ac.id

Abstract: Biomass is a material that can be potentially used as a natural fiber resource. Rice husk (RH) and sugarcane bagasse (SB), respectively containing 36.6% and 60% cellulose, are fibers that have the potential for biocomposite formation. In this study, an amine magnetic biocomposite (B-MNH₂) was prepared by a one-step solvothermal reaction. Delignified RH and SB fibers at a ratio of 1:1 were added to a mixture of ethylene glycol, iron chloride, and 1,6-hexanediamine, and kept in a stainless steel autoclave reactor at 200 °C for 6 h. The obtained B-MNH₂ contained 64.5% of Fe and 2.63 mmol/g of amine. Its surface area increased significantly from 9.11 m²/g to 25.81 m²/g after amine functionalization, and its optimum adsorption for Pb(II) ions was achieved within 360 min at 596.82 mg/g and pH 5. Moreover, the pseudo-first-order mechanism fitted well to the adsorption model. Other parameters, such as chemical oxygen demand (COD), total suspended solid (TSS), and dye during adsorption were also reduced by about 67.7%, 95.6%, and 89%, respectively. B-MNH₂ showed a slight decrease in performance by only 8% after the fourth repeated use. The amine magnetic biocomposite led to the development of a potential adsorbent due to the high surface area, stable material, and easy separation, and was capable of absorbing contaminants from an aqueous solution.

Keywords: biocomposite; Pb(II) ion; amine magnetic; rice husk; sugarcane bagasse; solvothermal



Citation: Nata, I.F.; Irawan, C.; Putra, M.D.; Wijayanti, H.; Dewi, Y.S.; Meliana, Y. A Sustainable Amine Magnetic Biocomposite Based on Rice Husk–Sugarcane Bagasse Fiber for Lead and Contaminant Adsorption in Aqueous Solution. *Magnetochemistry* **2022**, *8*, 183. <https://doi.org/10.3390/magnetochemistry8120183>

Academic Editors: Chuanliang Zhao, Bo Hu and Liwei Yang

Received: 31 October 2022

Accepted: 24 November 2022

Published: 9 December 2022

Publisher's Note: MDPI stays neutral with regard to jurisdictional claims in published maps and institutional affiliations.



Copyright: © 2022 by the authors. Licensee MDPI, Basel, Switzerland. This article is an open access article distributed under the terms and conditions of the Creative Commons Attribution (CC BY) license (<https://creativecommons.org/licenses/by/4.0/>).

1. Introduction

South Kalimantan has a typical type of rice called “Beras Banjar” as one of their largest agricultural products. Biomass waste as rice husk (RH) resulted from the utilization of paddy containing cellulose at approximately 34.34–43.80% [1]. Sugarcane bagasse (SB) is another organic material that is rich in cellulose at about 35.3–45.5% [2]. Biomass wastes produced from agricultural activities can affect the environment. Biomass wastes, such as rice husk, are used to either compress soft soil, or they are just burned, which could also later lead to air pollution. Sugarcane bagasse, on the other hand, is generally used for animal feed [3], paper making, and in inseminators as fuel. The possibility of exploring the fibers of these materials is interesting. Fibers are good materials for biocomposites since they have a matrix structure that provides them with a high surface area and high-performance of physical properties [4]. Both these materials are natural fibers that have potential as materials for biocomposite production. In addition, biomass waste is applied to a wide range of applications, not only for having a good specific strength, but also for being lightweight, environmentally friendly, and abundant in nature [5]. Based on the biomass technology approach, isolated fibers could be collected from biomass through a delignification process. RH and SB fibers were applied as a matrix to a biocomposite as

an adsorbent for ion removal in an aqueous solution. To enhance the functionality of the fibers, surface modification was carried out by depolymerization of the lignin, chemical treatment techniques, hemicellulose hydrolyzation, and disturbing the covalent bonds between the lignocellulosic components [6]. The chemical treatment of lignocellulose was conducted using an aqueous sodium hydroxide solution [7]. Many researchers have reported biomass fiber utilization, including the mechanical and physical properties of materials, specific for adsorbents for dye adsorption [8]; metal ions of Cu(II), Cd(II) [9], and chromium [10,11]; and Pb(II) ion [12] and Fe(III) ion adsorption [13]. Further studies have shown that the combination of carbon and sugarcane bagasse fiber as an adsorbent was capable of absorbing dye in a solution [14].

Several studies have been conducted to reduce the concentration of Pb(II) ions [15] and other heavy metal ions in aqueous solutions [16,17] by using magnetic nanoparticles as adsorbents. This is possible due to the high specific surface area of Fe₃O₄ particles created by modifying the amine groups. In addition, the advantages of using magnetic nanoparticles on biocomposite are the strong magnetic properties that make the material reusable and separation easy [18]. However, studies on the enhancement of the biocomposite activity by variation of natural fiber sources, especially biomass waste, are limited. The development of the preparation of magnetic nanoparticles by a one-step process by modifying the surface functional group in the biocomposite in the presence of rice husk fiber was investigated in [1,19], which focused on the preparation of an amine magnetic biocomposite based on the combination composition of RH and SB fiber. The characteristics of biocomposite, such as surface morphology, functional groups, crystalline structure, surface area, and thermal analysis, were observed. The kinetics and isotherm performance studies of amine magnetic biocomposite on Pb(II) ion adsorption, the effect on chemical oxygen demand (COD), total suspended solid (TSS), dye during adsorption, and reusability of adsorbent, were also investigated.

2. Materials and Methods

2.1. Materials

Rice husk (RH) and sugarcane bagasse (SB) were collected at Gambut and Banjarbaru, South Kalimantan, Indonesia. The Sasirangan textile wastewater at Banjarbaru, which contains dye, was used as a sample for adsorption. The Sasirangan textile wastewater contains TSS, COD, and dye at about 1.14 mg/L, 86.81 mg/L, and 0.99 absorbance values at 320 nm (three-time dilution), respectively. 1,6-Hexanediamine (C₆H₁₂N₂), ethylene glycol (C₂H₆O₂), iron(III) chloride hexahydrate (FeCl₃·6H₂O), sodium hydroxide (NaOH), sodium acetate anhydrous (C₂H₃NaO₂), ethanol (C₂H₆O), and hydrochloric acid (HCl) were purchased from Sigma Aldrich (Sigma-Aldrich Pte. Ltd, Singapore). All chemicals were of analytical grade and were used without purification.

2.2. Rice Husk and Sugarcane Bagasse Delignification Process

The RH and SB were washed with tap water to clean and remove impurities and dried in an oven at 80 °C for 24 h. Each material was blended into powder and sieved through a ±60 mesh. Then, RH and SB were kept in 1% NaOH (40% v/v) and heated at 80 °C with stirring at 100 rpm for 2 h. The solid part of the mixture was washed with deionized (DI) water until the filtrate reached pH~7 and kept again for 3 h at 80 °C. The delignified RH and SB were denoted as RH-D and SB-D, respectively.

2.3. Preparation of the Amine Magnetic Biocomposite Based on Rice Husk and Sugarcane Bagasse Fiber

The solvothermal method was applied to produce the amine magnetic biocomposite by a one-step process [19]. Briefly, 24 mL of ethylene glycol, 1.6 g of anhydrous sodium acetate, 0.8 g of iron(III) chloride hexahydrate, and 7 mL of 1,6-hexanediamine were mixed and heated at 50 °C while stirring at 150 rpm for 15 min. In the first 5 min, 0.5 g of fiber (RH-D and SB-D with a ratio of 1:1) was added to the mixture. After the time

was reached, the mixture was placed into the solvothermal reactor/Teflon stainless steel autoclave before being kept at 200 °C for 6 h. Once the reaction was completed, the reactor was cooled at room temperature until the product was ready to be taken out. The black solid material was washed with DI water, then 50% of ethanol was used 3 times each to remove any unreacted chemicals. The product was called as B-MNH₂. The preparation of biocomposite was signed in two types in which other biocomposite was prepared without 1,6-hexanediamine (B-M). B-M was used as a control for investigating the reactivity effect of amine functionalization on the biocomposite. B-M and B-MNH₂ were kept in DI water for the next experiment.

2.4. Simultaneous Adsorption of Pb(II) ions, Chemical Oxygen Demand (COD), Total Suspended Solid (TSS), and Dye of the Amine Magnetic Biocomposite

Adsorption studies of the biocomposite were carried out in a batch experiment. The Pb(II) ion solution was prepared from the dilution of Sasirangan textile wastewater with an initial concentration of 100 mg L⁻¹. The contact time effect (5, 15, 30, 60, 120, 240, 360, and 480 min) and pH (5, 7, and 9) of the solution were observed. The pH value was set using 0.1 M NaOH solution.

A 200 mL sample of Pb(II) ion solution was added with 60 g of biocomposite (B-M and B-MNH₂). Then, the mixture was shaken at room temperature for 150 rpm to obtain the optimum adsorption capacity condition. After the adsorption process, the biocomposite was collected by an external magnetic field, and the Pb(II) ion concentration remaining in solution was tested by atomic adsorption spectrophotometry (AAS). Data were collected in duplicate to obtain an average value. The repeated use of biocomposite was observed by the desorption of Pb(II) ion-loaded B-M and B-MNH₂ in 0.1 N HCl under 150 rpm for 4 h. Once the desorption time was reached, the biocomposite was washed with DI water until a pH of ~7 was obtained, and the regenerated B-M and B-MNH₂ was used as the adsorbent for the next run. The capacity of adsorption of Pb(II) ions was calculated by:

$$q_e = (C_o - C_e) \frac{V}{m}, \quad (1)$$

where C_o (mg L⁻¹) is the Pb(II) ion initial concentration, C_e (mg L⁻¹) is the Pb(II) ion equilibrium concentration, V (L) is the solution volume, and m (g) is the adsorbent amount.

2.5. Characterization of Material

Field-emission scanning electron microscopy (FE-SEM, JOEL JSM-6500F, JOEL LTD, Tokyo, Japan) was used to observe the morphological structure of all materials; samples were sputter-coated with platinum. Detection of elements on the sample was conducted using energy-dispersive X-ray fluorescence (XRF, Shimadzu Corporation, Kyoto, Japan) at 77 UA current and 20 kV voltage. The functional groups on samples were identified by Fourier transform infrared spectrometry (FT-IR, Bio-Rad, Digilab FTS-3500, SpectraLab Scientific Inc., Markham, ON, Canada). X-ray diffraction (XRD, Thermo Fisher Scientific Inc., Oxford, UK) was performed using copper k-alpha (CuK α) radiation on a Rigaku D/Max-B XRD machine at 100 mA current and 400 kV voltage.

The crystalline index (CrI) was calculated as follows:

$$\text{CrI} = \frac{I_{002} - I_{\text{am}}}{I_{002}}, \quad (2)$$

where CrI is the crystalline index (%), I_{am} is the intensity of amorphous part and I_{002} is the intensity of the crystal part. An Autosorb-1 instrument was used to measure the Brunauer–Emmet–Teller (BET) surface area of the material with the N₂ adsorption–desorption technique using a Quantachrome machine. The magnetic saturation value of naked magnetite particles and the biocomposite was investigated by a superconducting quantum interference device (SQUID, LakeShore 7307, Lake Shore Cryotronics, Inc., Westerville, OH, USA) magnetometer. Thermal gravimetric analysis (TGA) was used to observe the material

decomposition (Diamond TG/DTA, Perkin Elmer Inc., Waltham, MA, USA) in N₂ gas with a flow of 10 °C/min at 30–1000 °C. The decomposition of material components was studied by mass reduction from the curves of TGA.

2.6. Analysis

The amount of amine group, which was deposited on the surface of the biocomposite, was calculated by retro-titration [20]. Briefly, 100 mg of sample was dropped into 100 mL of 0.01 M HCl, and then the mixture was stirred for 2 h at 300 rpm. A 20 mL sample of supernatant collected by separation was titrated with 0.01 N NaOH. The concentration of amine group was calculated using the equation:

$$C_{\text{NH}_2} = \left[\frac{(C_{\text{HCl}} \times V_{\text{HCl}}) - (5C_{\text{NaOH}} \times V_{\text{NaOH}})}{m_{\text{sample}}} \right], \quad (3)$$

where m is the weight of the sample (g), C_{NaOH} is the concentration of NaOH (mmol L⁻¹), V_{NaOH} is the volume of NaOH (L), C_{HCl} is the concentration of HCl (mmol/L) and V_{HCl} is the volume of HCl (L).

The titrimetric permanganate method was used for COD analysis. Wastewater (100 mL) was mixed with 6 N H₂SO₄ (1 mL) and 0.01 N KMnO₄ (10 mL). Once homogenous, the mixture was heated up to the boiling point and cooled down to room temperature for about 10 min. A 0.01 N C₂H₂O₄·2H₂O (10 mL) sample was added and titrated by 0.01 KMnO₄ until the color of the solution turned pink. The titration was continued until the purple color disappeared. As a control, DI water was used for the blank solution, which was also titrated by 0.01 KMnO₄. The COD concentration in solution was calculated by:

$$\text{COD} \left(\frac{\text{mg}}{\text{L}} \right) = \left[\left((a + b) \times C_{\text{KMnO}_4} \right) - \left((V \times C)_{\text{C}_2\text{H}_2\text{O}_4} \right) \right] \times 8000, \quad (4)$$

where a is the volume of KMnO₄ titration standardization, b is the titration volume of KMnO₄, C_{KMnO_4} is the solution concentration (N), and $V_{\text{C}_2\text{H}_2\text{O}_4}$ (L) and $C_{\text{C}_2\text{H}_2\text{O}_4}$ are the volume and concentration of C₂H₂O₄ (N), respectively.

The Standard Test Method for Filterable and Nonfilterable Matter in Water was analyzed for TSS. The measured volume of textile wastewater containing Pb(II) ions was filtered through a pre-weighed glass fiber filter. The fiber filter was heated at 104 ± 1 °C until the mass became constant. TSS was calculated by:

$$\text{TSS} \left(\frac{\text{mg}}{\text{L}} \right) = \frac{(A - B) \times 100}{C}, \quad (5)$$

where A is the residue and filter dry weight (mg), B is the filter dry weight (mg), and C is the textile wastewater volume (L). The concentration of dye was observed by absorbance intensity, tested by UV-Vis spectroscopy (V-550, Jasco International Co., Ltd., Tokyo, Japan) at a wavelength of 320 nm as the maximum color adsorption on Sasirangan textile wastewater.

3. Results and Discussion

3.1. Amine Magnetic Biocomposite Characterization

Rice husk (RH) and sugarcane bagasse (SB) have a different characterization of structure morphology, crystals, functional groups, and thermal degradation. The delignification process changed the color and structure of RH and SB. The original color of RH and SB was brown and became lighter after treatment (Figure 1, inset). The color change was due the breaking of the lignocellulose structure by NaOH during treatment [21]. Based on FE-SEM observations, the surface morphology of rice husk was found to be rough and coated by lignin (Figure 1A). After treatment (Figure 1B), the surface became rougher and some pores were found on the surface. It is well known that RH contains silica plate at conical protrusions and bright spots at regular space. The increasing roughness of surface will increase the crack of conical protrusions because of the NaOH treatment. For SB

(Figure 1C), a smooth surface was observed, and then a rough surface was also found after treatment (Figure 1D). The RH and SB fibers were produced by delignification in the decomposition of lignin and hemicellulose. Those fibers were used as a matrix for magnetic nanoparticle growth.

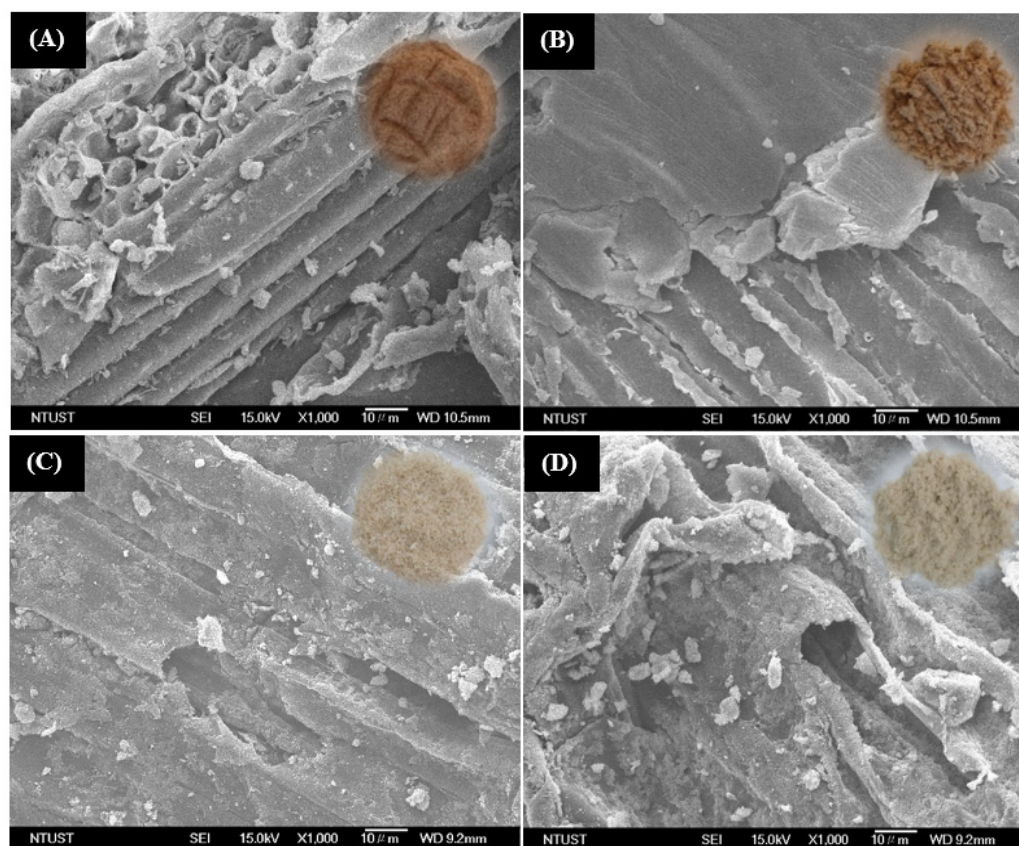


Figure 1. Morphology images of rice husk (RH) (A) before and (B) after delignification (RH-D), and sugarcane bagasse (C) before (SB) and (D) after delignification (SB-D).

Figure 2A shows the morphological structure of the amine magnetic biocomposite prepared by the combination of RH and SB in optimum conditions based upon our previous study [4]. The amine magnetic nanoparticle was grown and distributed on the fiber surface. This was confirmed by XRF analysis; the Fe content on B-M and B-MNH₂ was about 63.2% and 64.5%, respectively. The amine magnetic biocomposite (Figure 2B, inset) had a smaller size (± 50 nm) than the biocomposite prepared without amine (Figure 2A, inset). 1,6-Hexanediamine as an amine source for functionalization would prevent the magnetic growth, and amine functionalization could make the particles more reactive and stable [22]. The particle size of magnetic nanoparticles was almost twice smaller than that without amine in the synthesis of the biocomposite (Figure 2B, inset). In addition, the amount of fiber in the biocomposite also brought an effect on the amount of magnetic nanoparticle formation. This study applied the optimum amount and ratio of two kinds of fibers in the preparation, based on previous studies. The amine content on B-MNH₂ was detected to be about 2.63 mmol/g.

Biocomposite formation is also related with the mechanical properties of the fiber. The bulk density number of RH and SB is 1200 kg/m³ [23] and 300 kg/m³ [24], respectively. A good fiber composition ratio between RH and SB is 1:1, providing a template for the formation of amine magnetic nanoparticles [4]. The delignification process is specifically identified using the crystalline structure of the fiber. The RH and SB cellulose crystal structure can be identified using the crystalline index (CrI) value by XRD measurements. The specific peak for cellulose crystal is located at $2\theta = 20\text{--}80^\circ$ [25], and the amorphous

part shows wide diffraction at $2\theta = 0^\circ\text{--}20^\circ$ [26]. The characteristic peak of lignocellulose contains amorphous cellulose at 16.0° (cellulose I) and cellulose in its crystal form at 22.2° (cellulose II) (Figure 3). Delignification with NaOH solution significantly increased the crystal structure of RH and SB fibers by about 132% and 90.3%, respectively (Table 1). This proved that the delignification broke the lignin structure on lignocellulose. The formation of crystalline cellulose on the fiber due to the increase in the crystal peak intensity and the amorphous peak showed a reduction of the polysaccharide structure, as shown by a broad peak. The crystalline and amorphous peaks were taken as a measure of organized crystalline cellulose and the lack of organized polysaccharide structure [27]. The apparent magnetic particle on the sample can also be identified by XRD. As shown in Figure 3A, the specific peaks for magnetite were at 36° , 43° , and 57° (JCPDS card No. 39-0664), proving the formation of the magnetic particle in the biocomposite.

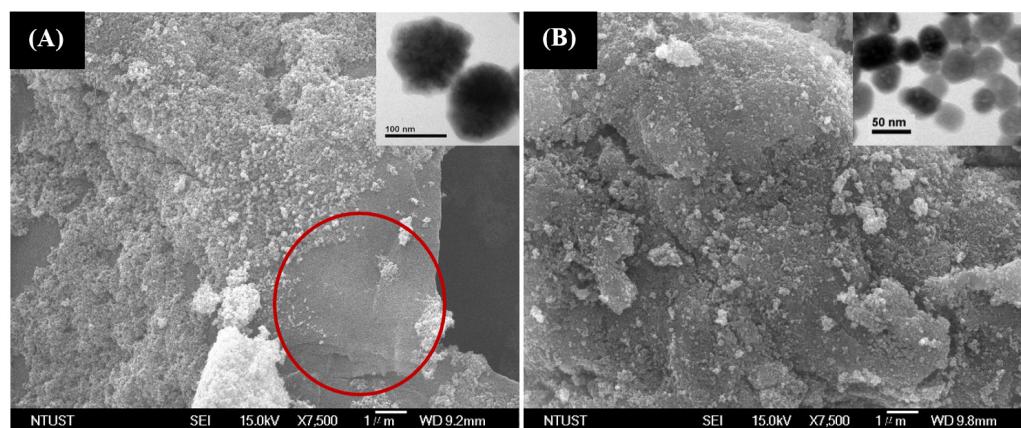


Figure 2. FE-SEM images of (A) magnetic biocomposite (B-M), the red circle indicates less magnetic area; and (B) amine magnetic biocomposite (B-MNH₂).

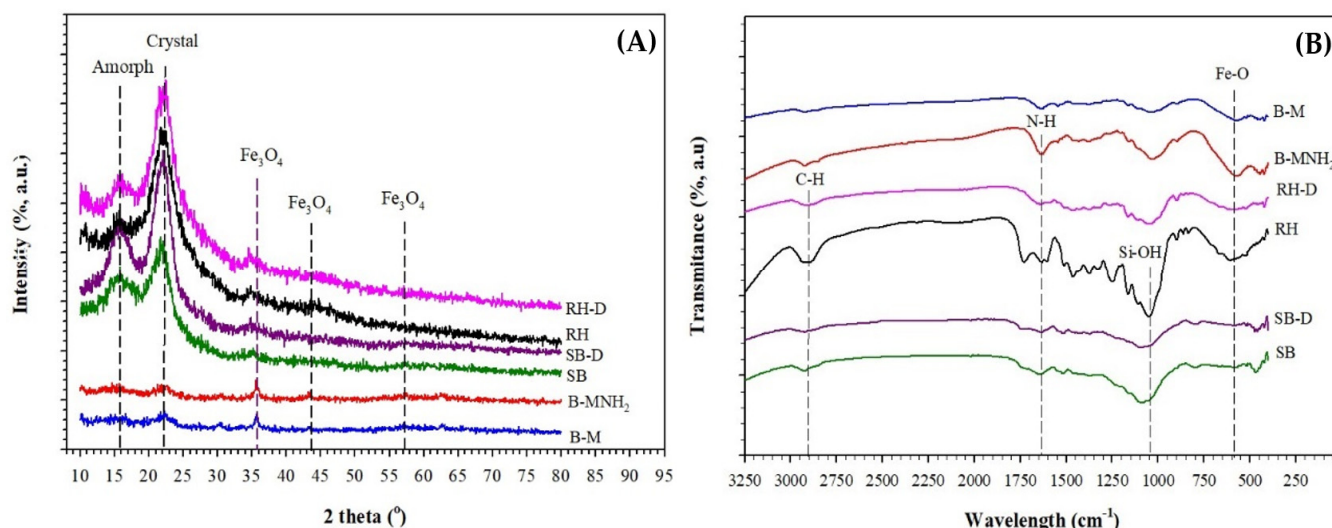


Figure 3. (A) X-ray diffraction (XRD) spectra and (B) FT-IR spectra of rice husk (RH), delignified rice husk (RH-D), sugarcane bagasse (SB), delignified sugarcane bagasse (SB-D), magnetic biocomposite (B-M), and amine magnetic biocomposite (B-MNH₂).

Figure 3B shows the FT-IR spectra of RH, RH-D, SB, SB-D, B-M, and B-MNH₂. The vibration spectra at 582 cm^{-1} showed Fe-O in the Fe₃O₄ stretching band for the biocomposite sample, and this peak did not appear on RH-D and SB-D. The modification of amine groups on the biocomposite surface for the N-H bending vibration was confirmed by the

peak at 1640 cm^{-1} . Another peak of RH and RH-D for the C-H stretching is shown at 2920 cm^{-1} . Only the peak at 1050 cm^{-1} was detected for the Si-OH band [1].

Table 1. Characteristic peaks of rice husk (RH), delignified rice husk (RH-D), sugarcane bagasse (SB), delignified sugarcane bagasse (SB-D).

Material	Characteristic Peak		CrI (%)
	Amorph (16.0°)	Crystal (22.4°)	
RH	771	1208	33.3330
RH-D	686	1218	77.551
SB	464	665	43.319
SB-D	564	1029	82.447

B-MNH₂ containing magnetite (Fe₃O₄) has super-paramagnetic properties. Due to this, the biocomposite is able to respond to an external magnetic field and facilitate the separation. The saturation magnetization of magnetite particles and biocomposite was performed by SQUID analysis at room temperature. Figure 4A shows the ferromagnetic behavior of naked amine magnetic nanoparticles (M), B-M, and B-MNH₂. The values of magnetic saturation of M, B-M, and B-MNH₂ were found at 67.94 emu/g, 30.49 emu/g, and 24.27 emu/g, respectively. The saturation value of the amine magnetic biocomposite was decreased by about 55.1%; this was probably due to the existence of RH and SB in the materials. A similar result was also obtained for a magnetic biocomposite based on rice husk [28,29] and sugarcane bagasse fiber [19].

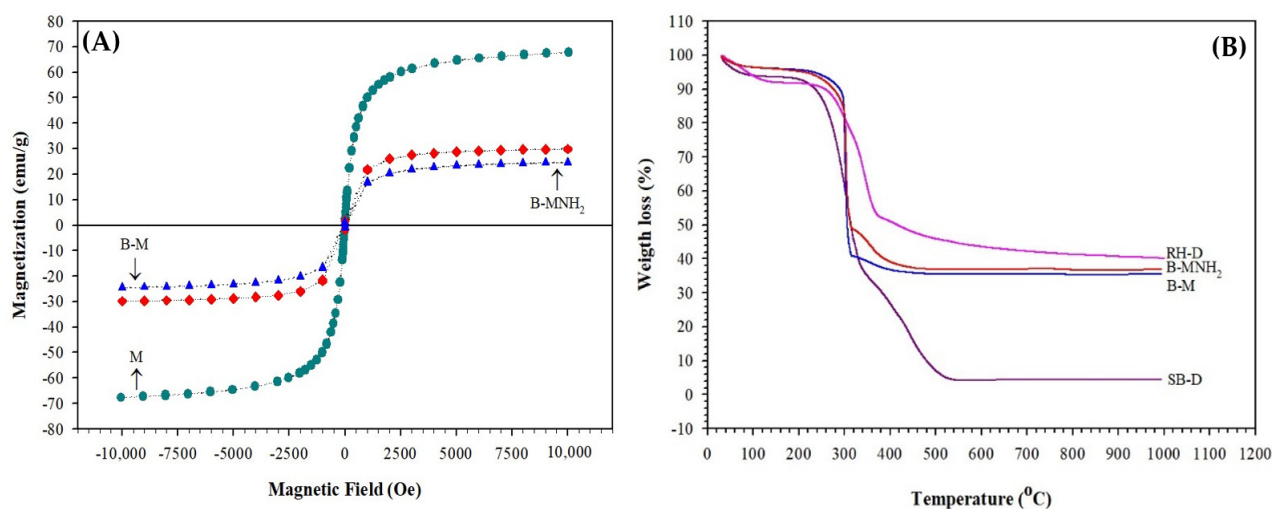


Figure 4. (A) Magnetization properties of naked amine magnetic nanoparticles (M), magnetic biocomposite (B-M), and amine magnetic biocomposite (B-MNH₂) at room temperature; (B) TGA analysis of delignified rice husk (RH-D), delignified sugarcane bagasse (SB-D), magnetic biocomposite (B-M), and amine magnetic biocomposite (B-MNH₂).

TGA thermograms of RH-D and SB-D showed a slight decrease in weight at 100–220 °C and 100–260 °C, respectively (Figure 4B). The weight loss was due to the decomposition of water and other volatile components. RH-D had a two-stage thermal degradation, occurring at a temperature range of 220–340 °C for the first stage, and at a temperature range of 340–800 °C for the second stage, in which the weight loss was up to 60.3%. SB-D also had a similar trend, in which the first stage was at a temperature of 260–380 °C and the second stage was at a temperature of 380–800 °C, with weight loss up to 95%. This weight loss occurred due to the decomposition of organic molecules of cellulose, hemicellulose and lignin of SB-D and RH-D [19].

Based on the thermogram analysis, B-MNH₂ was found to be more stable compared to B-M at 100–200 °C, in which a weight loss of about only 4% occurred. For further observation, the second stage occurred at 320 °C for both biocomposite. Interestingly, the remaining material of B-M and B-MNH₂ showed a weight loss of about 52% and 58%, respectively, indicating that the amine group on B-MNH₂ made the material stable at higher temperature compared to B-M. Furthermore, the biocomposite was quite stable at a temperature of 480 °C. The remaining residual of the amine biocomposite was about 37.8% higher than that of the remaining residual of B-M. The combination of fiber resource also affected the thermal stability of the biocomposite. The amine magnetic biocomposite, which only used SB-D as the fiber source, had a remaining residual of about 34.8% at the same temperature [19].

3.2. Kinetics Study of Pb(II) Ion Adsorption Using the Amine Magnetic Biocomposite as an Adsorbent

The kinetics of Pb(II) ion adsorption using amine magnetic biocomposite is deemed important to study, because the effects of the capacity and stability of the adsorbent will promote development. To determine the effectiveness of amine group functionalization on the biocomposite, biocomposite without amine functionalization was prepared as well. Adsorption kinetics, including pseudo-first-order and pseudo-second-order models, were applied to study the kinetic models following the equations [30,31]:

$$Q_t = Q_e \left(1 - e^{-k_1 t}\right), \quad (6)$$

$$\frac{t}{Q_t} = \frac{t}{Q_e} + \frac{t}{k_2 Q_e^2}, \quad (7)$$

where Q_e (mg/g) is the amount of Pb(II) ions adsorbed at equilibrium, Q_t (mg/g) is the amount of Pb(II) ions at time t , and k_1 (min⁻¹) and k_2 (g mg⁻¹ min⁻¹) are the rate constant of pseudo-first-order and pseudo-second-order models for the adsorption process, respectively.

Figure 5 shows the adsorption capacity profile of Pb(II) ions with B-M and B-MNH₂. Both types of adsorbent can bind with Pb(II) ions with a significant adsorption capacity during first 120 min. The increasing adsorption capacity was related to the high concentration of Pb(II) ions at the beginning of adsorption and the high availability of empty sites of the adsorbent.

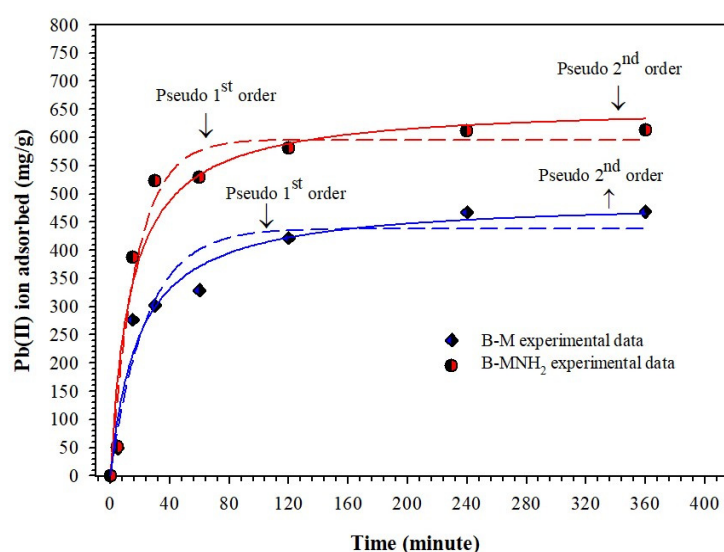


Figure 5. Kinetic Pb(II) ion adsorption by B-M and B-MNH₂ at different contact times. Reaction conditions: an initial Pb(II) ion concentration of 100 mg L⁻¹, an adsorbent mass of 60 mg, a sample volume of 200 mL, a pH of 5, and a shaking rate of 150 rpm.

For a longer contact time, the adsorption capacity became constant after reaching the equilibrium time, due to the saturation conditions of the adsorbent when its surface was filled with Pb(II) ions. The adsorption equilibrium of Pb(II) ions by B-M and B-MNH₂ was achieved at 360 min.

The adsorption process using B-M as the adsorbent at pH 5 led to a change of the magnetic surface into the deprotonated form FeO⁻. The adsorption of Pb(II) ions occurred due to the negative charge of the BM surface and electrostatic interaction [32]. This study showed that amine functionalization on the biocomposite (B-MNH₂) surface enhanced the adsorption capacity due to the formation of NH³⁺, and the positive surface charge of amine magnetic biocomposite was stable. In addition, the water solubility of amine brought an effect on the increase in the hydrogen bonding, as well as the lone electron pair. The higher activity to capture the Pb(II) ions occurred in this condition [19,29]. This confirmed that the amine magnetic biocomposite had a significant effect on adsorption capacity. On the other hand, the surface area also significantly increased for B-M and B-MNH₂ from 9.11 to 25.81 m²/g, respectively. This result was confirmed by FE-SEM and TEM analysis, in which B-MNH₂ had a smaller particles size (around ± 50 nm), a high permeability, and stable mechanical and thermal properties, so that the adsorption process could run well [33]. B-MNH₂ surface area was 2.83-fold higher than that of SB-M.

Table 2 shows the results of the kinetics adsorption fitting data. The adsorption kinetics of Pb(II) ions by B-M followed the pseudo-second-order kinetics model, with an R² value of 0.981 and a Q_e value of 489.578 mg/g. The B-M adsorption kinetics model assumed that the interaction between the adsorbent and the adsorbate occurred by chemical reactions and ion exchange [34], similar to the results of other studies [35]. On the other hand, B-MNH₂ was retrieved with a pseudo-first-order kinetics model, with an R² value of 0.981 and an Q_e of 596.23 mg/g, and this adsorption process was controlled by physical adsorption. The pseudo-first-order adsorption mechanism assumed that ion entrapment on van der Waals appears between molecule ions from the adsorbate solution onto the adsorbent surface. In other words, the control step of the adsorption rate was a chemical potential gradient between the Pb(II) ions and the adsorbent surface. In addition, the activity of the adsorbent site would have a strong interaction with metal ions with a smaller k value; then adsorption can occur faster and more efficiently [35]. The adsorption capacity of B-MNH₂ was about 21.8% higher than that of B-M. This was related to the amine group on B-MNH₂, and it affected the surface charge of the biocomposite to be positive (-NH³⁺).

Table 2. Kinetic parameters of Pb(II) ion adsorption using B-M and B-MNH₂ as an adsorbent.

Adsorbent Type	Parameter	Kinetics Model	
		First Order	Second Order
B-M	Q _e (mg/g)	438.22	489.58
	k ₁ (s ⁻¹)	0.0098	0.00003
	R ₂	0.969	0.981
B-MNH ₂	Q _e (mg/g)	596.23	657.46
	k ₁ (s ⁻¹)	0.057	0.00004
	R ²	0.982	0.973

3.3. Adsorption Isotherm Study of Pb(II) Ions Using the Amine Magnetic Biocomposite as an Adsorbent

The adsorption isotherm can be used to evaluate the adsorption capacity of the adsorbent for heavy metal ion separation from a solution. This process shows the equilibrium conditions of adsorbent, which reacts with metal ion in the solution [36]. Isotherm studies were carried out in various concentrations of Pb(II) ions in the range of 20–250 mg/L. At low Pb(II) ion concentration, all Pb(II) ions interacted with active site on the adsorbent surface, whereas at higher initial concentrations, the adsorption concentration site became saturated and the adsorption capacity decreased [12]. The initial concentration provided the driving force required to surmount the resistance to mass transfer of metal ions between

the water phase and the solid phase [15]. Therefore, increasing the initial concentration also increased metal ion uptake. The adsorption data were analyzed using Langmuir (Equation (8)) and Freundlich (Equation (9)) isotherms with the following equations:

$$Q_e = \frac{Q_0 b C_e}{1 + b C_e} \quad (8)$$

$$Q_e = K_f \cdot C_e^{1/n} \quad (9)$$

For the Langmuir model, Q_e is the number of metal ions adsorbed per gram of adsorbent at equilibrium (mg/g), Q_0 is the maximum adsorption capacity (mg/g), C_e is the ion concentration in solution at equilibrium (mg/L), and b is the Langmuir biosorption constant (L/mg). For the Freundlich model, K_f is the adsorption capacity constant ($\text{mg mg}^{-1/n} \cdot \text{L/g}$) and $1/n$ is a constant describing the adsorption intensity. Figure 6 shows the adsorption isotherm of Pb(II) by B-M and B-MNH₂. The maximum adsorption capacity of B-M and B-MNH₂ for Pb(II) ions was 1562.18 mg/g and 717.6 mg/g, respectively. Here, the Langmuir model provided the best fit to the equilibrium adsorption data.

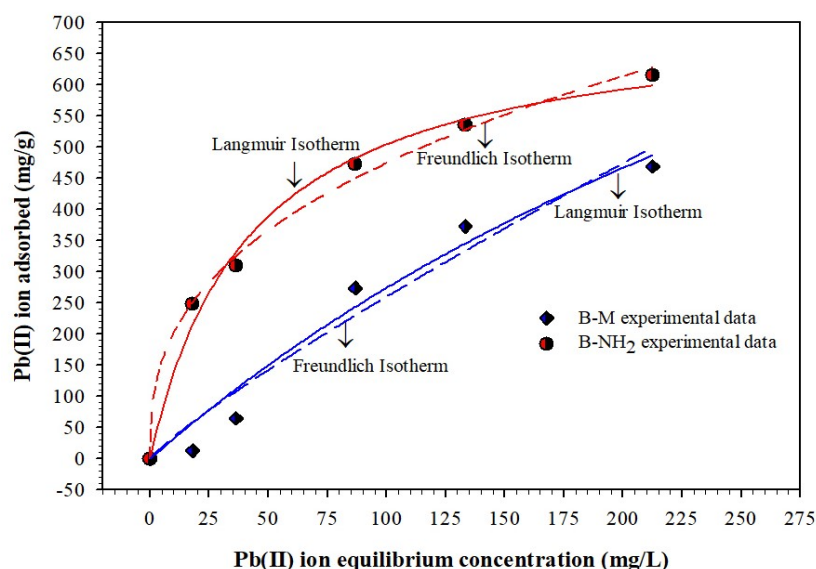
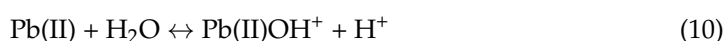


Figure 6. Isotherm study of Pb(II) ion adsorption by B-M and B-MNH₂. Reaction conditions: an adsorbent mass of 60 mg, a sample volume of 200 mL, a pH of 5, and a shaking rate of 150 rpm.

Table 3 shows the parameters (Q_0 , Q_e , b , K_f , n , and R^2) of two isotherm models. The adsorption of Pb(II) ions on B-M and B-MNH₂ fit well using the Langmuir adsorption isotherm model, with higher R^2 values. The results showed that the binding sites of adsorbents were uniformly distributed on the surface and adsorption of Pb(II) ions was considered as single layer adsorption. This is consistent with the research using adsorbents made from amine-modified sugarcane and magnetic fibers [15,37].

3.4. pH Effect on Pb(II) Ion Adsorption Capacity, Chemical Oxygen Demand (COD), Total Suspended Solid (TSS), and Dyes in Aqueous Solution Using the Amine Magnetic Biocomposite

The pH value in solution will affect the ion concentration in solution and the surface charge of the adsorbent; hence, it is important to study the pH of the solution for the adsorption profile. The Pb(II) ion adsorption can be determined by ion exchange, surface complex formation, or electrostatic interactions between Pb(II) ions and the surface of the adsorbent [38]. The effect of pH in the solution for the adsorption of Pb(II) ions is described in the following reaction:





The speciation of Pb(II) in water will form $\text{Pb(OH)(NO}_3\text{)}$, so not only does the binding of metal ions by adsorbents occur in metal atoms, but they can also bind with H atoms on -OH groups via hydrogen bonds. Figure 7A shows the Pb(II) ion adsorption with varying pH. The adsorption capacity for B-M and B-MNH₂ at pH 5 was 586.74 mg/g and 611.82 mg/g, respectively. The higher adsorption capacity of Pb(II) ions occurred at pH 5, and by increasing the pH value, the H⁺ ion reduced and the equilibrium shifted to the right of the reaction, so that the PbOH⁺ equilibrium increased.

Table 3. Pb(II) ion adsorption isotherm parameters using B-M and B-MNH₂.

Adsorbent Type	Adsorption Isotherm	Constant	Value
B-M	Langmuir	Q_e (mg/g)	1562.18
		b (L/mg)	0.0021
		R^2	0.9844
	Freundlich	n	4.8341
		K_f	1.1151
B-MNH ₂	Langmuir	Q_e (mg/g)	717.60
		b (L/mg)	0.0237
		R^2	0.9965
	Freundlich	n	85.827
		K_f	2.6910
		R^2	0.9963

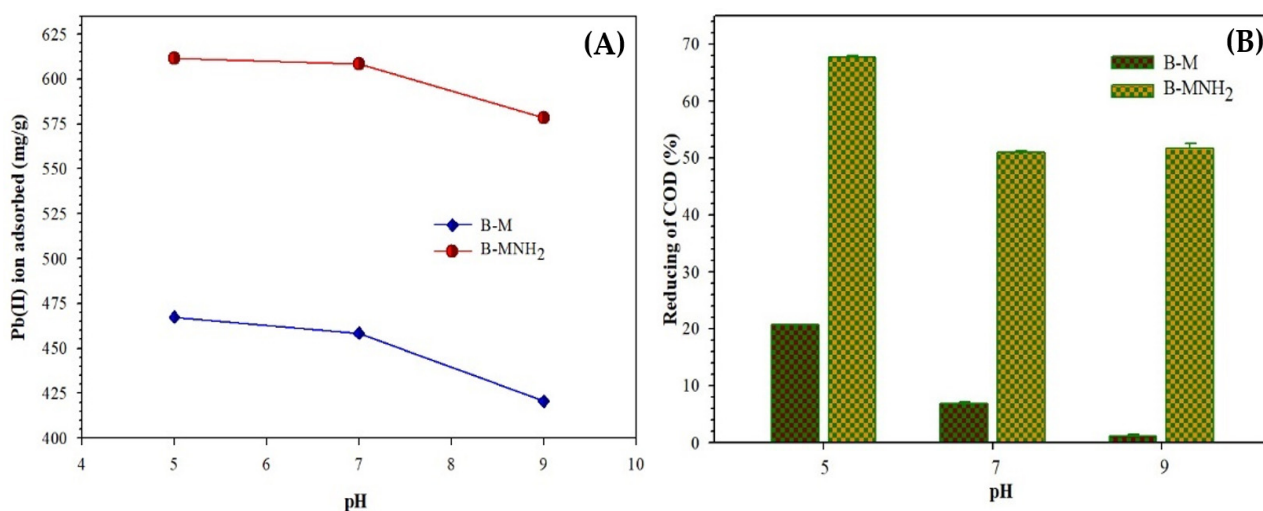


Figure 7. (A) Pb(II) ion adsorption capacity and (B) percentage of COD reduction of the adsorption process at varying pH with an adsorbent mass of 60 mg, a sample volume of 300 mL, and a stirring speed of 150 rpm for 360 min.

In addition, the adsorbent surface was negatively charged by releasing protons through electrostatic force. Furthermore, the capacity adsorption increased due to an attractive interaction between the adsorbate and the adsorbent. On the other hand, increasing the pH value caused the hydrogen ion concentration to gradually decrease and the adsorbent surface to deprotonate. For this condition, an interaction occurred between the Pb(II) ions and OH⁻ anions to form Pb(OH)_2 . For the alkaline condition, an oxide compound was formed from a larger impurity element to cover the surface of the adsorbent. The soluble Pb(OH)_2 species became dominant and precipitation of Pb(OH)_2 occurred at the value of pH above 6.5 [36]. In this study, a pH of 5 is the optimum condition for adsorption, which is in line with the results of other studies [13,19,22,29].

The adsorption capacity of B-M and B-MNH₂ were studied by comparing it with another adsorbent. Table 4 shows the adsorption capacity of different adsorbent containing magnetic particles. The biocomposite prepared by cellulose had good adsorption capacity toward the Pb(II) ions, which was about 4.6-fold higher than that of the magnetic particle chitosan functionalized by L-arginine.

Table 4. Maximum adsorption capacity of Pb(II) ion adsorption on different adsorbents.

Adsorbent Type	Adsorption Capacity (mg/g)	pH _e	Reference
Magnetic functionalized by polyethyleneimine	96.60	6	[39]
Amine bifunctionalized on MNPs	110.13	5	[40]
Magnetic chitosan functionalized by L-arginine	128.63	6	[41]
Rice husk magnetic biocomposites (RHB-M)	300.78	5	[29]
Rice husk amine magnetic (RHB-MH ₂)	680.19	5	[29]
Magnetic biocomposite based on rice husk and sugarcane bagasse (B-M)	489.58	5	This study
Amine magnetic biocomposite based on rice husk and sugarcane bagasse (B-MNH ₂)	596.23	5	This study

Another effect of pH during the adsorption was COD concentration, in which the adsorption mechanism was related with the surface charge of the adsorbent, stability, degree of ionization, and color intensity of compounds in aqueous solution [42]. The shaking treatment in the adsorption process facilitated the contact between the adsorbent and organic compounds in solution, so that it could also affect COD levels in wastewater. Figure 7B shows the COD reduction at various pH values; the largest reduction for B-M and B-MNH₂ occurred at pH 5 at a value of 20.7% and 67.7%, respectively. The COD initial concentration of wastewater was 86.81 mg/L. It is well known that the COD value decreases with the increase in the pH value. At higher pH, adsorption capacity is lower due to an increase in the diffusion barrier of organic ions as well as OH⁻ ions. This condition then induces competition between the organic molecules and the adsorbent surface [43]. At low pH, the organic molecules become positively charged and bound with the surface negative charge of the adsorbent by electrostatic interaction. The same behavior of the COD effect on pH has been shown in previous studies using adsorbent from biomass [19,44].

B-M and B-MNH₂ were also able to reduce TSS. The suspended particles were stable in solution, and could be neutralized by a destabilization process due to the positive charge formation of the adsorbent. Afterward, the energy resistance was reduced and started to flock formation. The positive charge on the adsorbent could also interact with negative charges of the surface of suspended particles, and this made the repulsion force between suspended particles weak. The reduction of the TSS profile is presented in Figure 8A. Again, the highest value of TSS reduced at pH 5, due to the positive charge formation of the adsorbent. The TSS was reduced by only about 2% in three different pH values, meaning that almost all of the TSS was adsorbed on the surface of the adsorbent. Besides COD and TSS, another effect during adsorption was dye reduction (Figure 8B). The highest dye reduction for B-M and B-MNH₂ occurred at pH 5. A dye reduction value of about 82.6% and 89% was obtained for B-M and B-MNH₂, respectively. Clear wastewater could be found after adsorption for both biocomposites at pH 5, as presented in Figure 7, inset.

The brown color of wastewater turned clear after adsorption. The dye reduction difference of about 20%, from pH 5 to 9, clearly described the amount of surface positive charge of the adsorbent at low pH. The decrease in the dye intensity might be due to protonation which enhances the electrostatic interaction between negatively charged anions of dye molecules and the surface of the positively charged adsorbent [45].

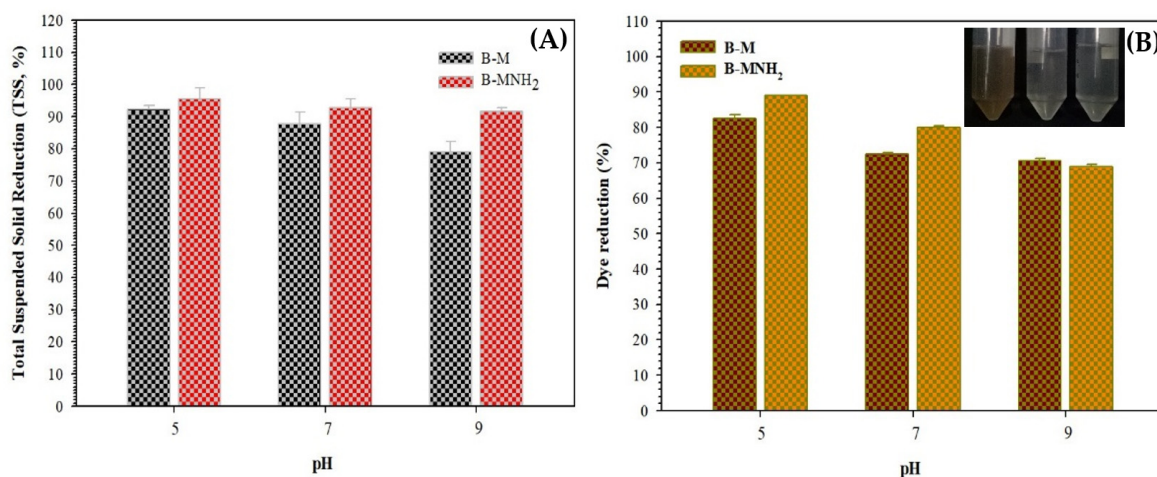


Figure 8. (A) TSS reduction and (B) dye reduction at different pH in the adsorption process with a sample volume of 300 mL, an initial Pb(II) ion concentration of 100 mg L⁻¹, an adsorbent mass of 60 mg, and a stirring speed of 150 rpm for 360 min.

3.5. Reusability Performance of Amine Magnetic Biocomposites for Pb(II) Ion Adsorption

Observing the regeneration of biocomposites is very important, and is in line with effectiveness, and economic and environmental aspects. The desorption of Pb(II) ions used 0.01 M HCl, which was selected as a better effluent for adsorbent reusability, up to 91% desorption [46]. At low pH, the hydrogen ion was bound with ligand, and then desorption of Pb(II) ions occurred. The desorption process allowed Pb(II) ions to bind to Cl⁻ to form PbCl₂. After washing with DI water, the adsorbent was ready to be used for the next process. As seen in Figure 9, the profile of Pb(II) ion adsorption capacity using B-M and B-MNH₂ was conducted in four cycles. The percentage desorption efficiency achieved for B-M and B-MNH₂ was about 91.1% and 91.6%, respectively. The performance of B-M and B-MNH₂ for reusability slightly decreased below 10% after the fourth cycle, i.e., 8.85% and 7.96%, respectively. A similar result was also seen for other biocomposite adsorbents [19,29]. The deviation of the value occurred due to the unalterable ion of the functional groups on the adsorbent surface, which decreased the number of available active sites between the adsorbate and the adsorbent, and weakened the electrostatic interaction between the two [47]. A slight reduction in adsorption capacity, due to incomplete desorption of divalent metal ions on the adsorbent surface and the reduction of surface functional groups, such as -OH and -NH₂ groups [48], occurred as well.

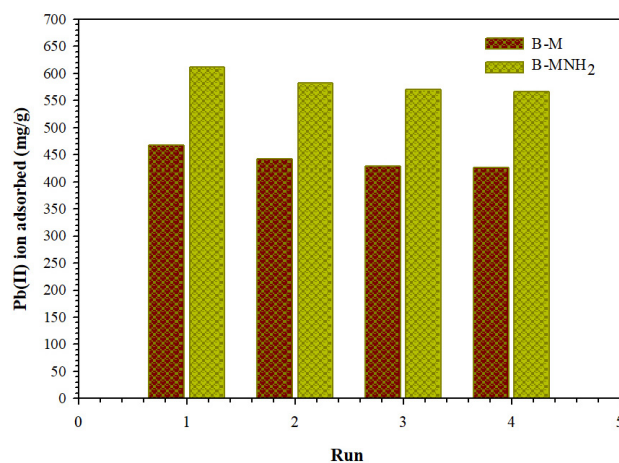


Figure 9. Repetition of the adsorbent in adsorption with a sample volume of 200 mL, an initial Pb(II) ion concentration of 100 mg L⁻¹, an adsorbent mass of 60 mg, a pH of 5, and a stirring speed of 150 rpm for 360 min.

This finding showed that amine magnetic biocomposite material is a potential reusable adsorbent. B-MNH₂ is more reactive in the adsorption process, including Pb(II) ion adsorption, and reduces the amount of COD, TSS, and dye in aqueous solution more than B-M, as well as the reusability of the biocomposite. The amine magnetic biocomposite is proven to be more effective and confirms that its capability as an adsorbent for a wide range of pollutants in aqueous solution.

4. Conclusions

The combination of rice husk and sugarcane bagasse fiber with the incorporation of magnetic nanoparticles forms a biocomposite. The biocomposite is a much more efficient adsorbent for the removal of Pb(II) ions and other contaminants, such as COD, TSS, and dye, from wastewater. Equilibrium adsorption was achieved at pH 5 within 360 min. The kinetics mechanism of Pb(II) ion adsorption followed the pseudo-first-order model and the maximum adsorption capacity reached up to 596.23 mg/g. The simultaneous adsorption also reduced number of COD, TSS, and dye by 67.7%, 95.6%, and 89%, respectively. The reusability of amine magnetic biocomposite was stable after the fourth repeated use. The amine magnetic biocomposite was found to be an attractive and promising alternative adsorbent for wastewater treatment and environmental contamination control.

Author Contributions: Conceptualization, C.I., M.D.P. and I.F.N.; methodology, H.W. and Y.M.; validation, Y.S.D. and C.I.; formal analysis, M.D.P., I.F.N., C.I. and Y.M.; investigation, M.D.P. and H.W.; writing—original draft preparation, I.F.N. and Y.S.D.; writing—review and editing, M.D.P., C.I. and Y.M.; supervision, I.F.N. All authors have read and agreed to the published version of the manuscript.

Funding: This research was funded through the World Class Research Project (026/E5/PG.02.00.PT/2022) and Graduate Research Project (113.1.12/UN8.2/PG/2020) by the Ministry of Education, Culture, Research and Technology (Kemendikbudristek), Republic of Indonesia.

Institutional Review Board Statement: Not applicable.

Informed Consent Statement: Not applicable.

Data Availability Statement: Not applicable.

Acknowledgments: The authors would like to express their gratitude to C.K. Lee (Taiwan Tech, Taipei, Taiwan) for support with FE-SEM and TEM observations.

Conflicts of Interest: The authors declare no conflict of interest.

References

1. Nata, I.F.; Putra, M.D.; Nurandini, D.; Irawan, C.; Fitriani, R.; Isnaini, M.D. Rice Husk Fiber Magnetic Nanoparticle Biocomposites: Preparation and Characterization. *IOP Conf. Ser. Earth Environ. Sci.* **2018**, *175*, 012005. [[CrossRef](#)]
2. Supranto, S.; Tawfiequrrahman, A.; Yunanto, D.E. Sugarcane Bagasse Conversion to High Refined Cellulose Using Nitric Acid, Sodium Hydroxide and Hydrogen Peroxide as the Delignification Agents. *J. Eng. Sci. Technol.* **2015**, *1*, 35–46.
3. Ilindra, A.; Dhake, J.D. Microcrystalline Cellulose from Bagasse and Rice Straw. *Indian J. Chem. Technol.* **2008**, *15*, 497–499.
4. Dewi, Y.S.; Wijayanti, H.; Lestari, R.A.; Nata, I.F. Preparation of magnetic nanoparticle biocomposites using rice husk and sugarcane bagasse fibers as the matrix. *IOP Conf. Ser. Mater. Sci. Eng.* **2020**, *980*, 012007. [[CrossRef](#)]
5. Hameed, B.H.; Ahmad, A.A. Batch adsorption of methylene blue from aqueous solution by garlic peel, an agricultural waste biomass. *J. Hazard. Mater.* **2009**, *164*, 870–875. [[CrossRef](#)]
6. Rokbi, M.; Osmani, H.; Imad, A.; Benseddiq, N. Effect of Chemical treatment on Flexure Properties of Natural Fiber-reinforced Polyester Composite. *Procedia Eng.* **2011**, *10*, 2092–2097. [[CrossRef](#)]
7. Karp, S.G.; Woiciechowski, A.L.; Soccol, V.T.; Soccol, C.R. Pretreatment strategies for delignification of sugarcane bagasse: A review. *Braz. Arch. Biol. Technol.* **2013**, *56*, 679–689. [[CrossRef](#)]
8. Guimarães Gusmão, K.A.; Alves Gurgel, L.V.; Sacramento Melo, T.M.; Gil, L.F. Application of succinylated sugarcane bagasse as adsorbent to remove methylene blue and gentian violet from aqueous solutions—Kinetic and equilibrium studies. *Dye. Pigment.* **2012**, *92*, 967–974. [[CrossRef](#)]
9. Zhang, Z.; Moghaddam, L.; O'Hara, I.M.; Doherty, W.O.S. Congo Red adsorption by ball-milled sugarcane bagasse. *Chem. Eng. J.* **2011**, *178*, 122–128. [[CrossRef](#)]

10. Dos Santos, V.C.G.; De Souza, J.V.T.M.; Tarley, C.R.T.; Caetano, J.; Dragunski, D.C. Copper Ions Adsorption from Aqueous Medium Using the Biosorbent Sugarcane Bagasse In Natura and Chemically Modified. *Water Air Soil Pollut.* **2011**, *216*, 351–359. [[CrossRef](#)]
11. Mahmood-ul-Hassan, M.; Suthar, V.; Rafique, E.; Ahmad, R.; Yasin, M. Kinetics of cadmium, chromium, and lead sorption onto chemically modified sugarcane bagasse and wheat straw. *Environ. Monit. Assess.* **2015**, *187*, 470. [[CrossRef](#)] [[PubMed](#)]
12. Hamza, I.A.A.; Martincigh, B.S.; Ngila, J.C.; Nyamori, V.O. Adsorption studies of aqueous Pb(II) onto a sugarcane bagasse/multi-walled carbon nanotube composite. *Phys. Chem. Earth Parts A/B/C* **2013**, *66*, 157–166. [[CrossRef](#)]
13. Nata, I.F.; Mirwan, A.; Wicakso, D.R.; Irawan, C.; Isnaini, M.D.; Fitriani, R. Adsorption of Fe³⁺ ion from Aqueous Solution onto Rice Husk Biocomposite Magnetic Nanoparticle. *IOP Conf. Ser. Earth Environ. Sci.* **2020**, *506*, 012006. [[CrossRef](#)]
14. Rattanachueskul, N.; Saming, A.; Kaowphong, S.; Chumha, N.; Chuenchom, L. Magnetic carbon composites with a hierarchical structure for adsorption of tetracycline, prepared from sugarcane bagasse via hydrothermal carbonization coupled with simple heat treatment process. *Bioresour. Technol.* **2017**, *226*, 164–172. [[CrossRef](#)] [[PubMed](#)]
15. Yu, J.-X.; Wang, L.-Y.; Chi, R.-A.; Zhang, Y.-F.; Xu, Z.-G.; Guo, J. Competitive adsorption of Pb²⁺ and Cd²⁺ on magnetic modified sugarcane bagasse prepared by two simple steps. *Appl. Surf. Sci.* **2013**, *268*, 163–170. [[CrossRef](#)]
16. Tan, Y.; Chen, M.; Hao, Y. High efficient removal of Pb (II) by amino-functionalized Fe₃O₄ magnetic nano-particles. *Chem. Eng. J.* **2012**, *191*, 104–111. [[CrossRef](#)]
17. Cui, Y.; Liu, S.; Hu, Z.-J.; Liu, X.-H.; Gao, H.-W. Solid-phase extraction of lead(II) ions using multiwalled carbon nanotubes grafted with tris(2-aminoethyl)amine. *Microchim. Acta* **2011**, *174*, 107. [[CrossRef](#)]
18. Hao, Y.-M.; Man, C.; Hu, Z.-B. Effective removal of Cu (II) ions from aqueous solution by amino-functionalized magnetic nanoparticles. *J. Hazard. Mater.* **2010**, *184*, 392–399. [[CrossRef](#)]
19. Irawan, C.; Putra, M.D.; Wijayanti, H.; Juwita, R.; Meliana, Y.; Nata, I.F. The Amine Functionalized Sugarcane Bagasse Biocomposites as Magnetically Adsorbent for Contaminants Removal in Aqueous Solution. *Molecules* **2021**, *26*, 5867. [[CrossRef](#)]
20. Nata, I.F.; Sureshkumar, M.; Lee, C.-K. One-pot preparation of amine-rich magnetite/bacterial cellulose nanocomposite and its application for arsenate removal. *RSC Adv.* **2011**, *1*, 625–631. [[CrossRef](#)]
21. de Carvalho Neto, A.G.V.; Ganzerli, T.A.; Cardozo, A.L.; Fávoro, S.L.; Pereira, A.G.B.; Giroto, E.M.; Radovanovic, E. Development of composites based on recycled polyethylene/sugarcane bagasse fibers. *Polym. Compos.* **2014**, *35*, 768–774. [[CrossRef](#)]
22. Irawan, C.; Nata, I.F.; Lee, C.-K. Removal of Pb(II) and As(V) using magnetic nanoparticles coated montmorillonite via one-pot solvothermal reaction as adsorbent. *J. Environ. Chem. Eng.* **2019**, *7*, 103000. [[CrossRef](#)]
23. Panthapulakkal, S.; Law, S.; Sain, M. Enhancement of Processability of Rice Husk Filled High-density Polyethylene Composite Profiles. *J. Thermoplast. Compos. Mater.* **2005**, *18*, 445–458. [[CrossRef](#)]
24. Qureshi, K.; Bhatti, I.; Kazi, R.; Ansari, A.K. Physical and chemical analysis of activated carbon prepared from sugarcane bagasse and use for sugar decolorisation. *Int. J. Chem. Biomol. Eng.* **2008**, *1*, 145–149.
25. Hashemian, S.; Hosseini, S.H.; Salehifar, H.; Salari, K. Adsorption of Fe(III) from Aqueous Solution by Linde Type-A Zeolite. *Am. J. Anal. Chem.* **2013**, *04*, 123–126. [[CrossRef](#)]
26. Mohadi, R.; Hidayati, N.; Lesbani, A. Adsorption Desorption of Chromium (III) Ion on Cellulose From Wood Powder. *Int. J. Sci. Eng. (IJSE)* **2014**, *7*, 77–80. [[CrossRef](#)]
27. Ghali, L.; Msahli, S.; Zidi, M.; Sakli, F. Effects of Fiber Weight Ratio, Structure and Fiber Modification onto Flexural Properties of Luffa-Polyester Composites. *Adv. Mater. Phys. Chem.* **2011**, *01*, 78–85. [[CrossRef](#)]
28. Zhang, X.; Kan, X.; Wang, M.; Rao, R.; Qian, N.; Zheng, G.; Ma, Y. Mechanism of enhanced magnetization in CoFe₂O₄/La_{0.7}Sr_{0.3}MnO₃ composites with different mass ratios. *Ceram. Int.* **2020**, *46*, 14847–14856. [[CrossRef](#)]
29. Nata, I.F.; Wicakso, D.R.; Mirwan, A.; Irawan, C.; Ramadhani, D.; Ursulla. Selective adsorption of Pb(II) ion on amine-rich functionalized rice husk magnetic nanoparticle biocomposites in aqueous solution. *J. Environ. Chem. Eng.* **2020**, *8*, 104339. [[CrossRef](#)]
30. Lagrergen, S. Zur Theorie Der Sogenannten Adsorption Gelöster Stoffe Kungliga Svenska Vetenskapsakademiens. *Handlingar* **1898**, *24*, 1–39.
31. Ho, Y.-S.; McKay, G. Pseudo-second order model for sorption processes. *Process Biochem.* **1999**, *34*, 451–465. [[CrossRef](#)]
32. Pipiška, M.; Zardňanská, S.; Horník, M.; Ďuriška, L.; Holub, M.; Šafařík, I. Magnetically Functionalized Moss Biomass as Biosorbent for Efficient Co²⁺ Ions and Thioflavin T Removal. *Materials* **2020**, *13*, 3619. [[CrossRef](#)] [[PubMed](#)]
33. Wu, W.; He, Q.; Jiang, C. Magnetic iron oxide nanoparticles: Synthesis and surface functionalization strategies. *Nanoscale Res. Lett.* **2008**, *3*, 397–415. [[CrossRef](#)] [[PubMed](#)]
34. Liu, W.; Zhao, C.; Wang, S.; Niu, L.; Wang, Y.; Liang, S.; Cui, Z. Adsorption of cadmium ions from aqueous solutions using nano-montmorillonite: Kinetics, isotherm and mechanism evaluations. *Res. Chem. Intermed.* **2018**, *44*, 1441–1458. [[CrossRef](#)]
35. Chu, Y.; Khan, M.A.; Wang, F.; Xia, M.; Lei, W.; Zhu, S. Kinetics and equilibrium isotherms of adsorption of Pb(II) and Cu(II) onto raw and arginine-modified montmorillonite. *Adv. Powder Technol.* **2019**, *30*, 1067–1078. [[CrossRef](#)]
36. Homagai, P.L.; Ghimire, K.N.; Inoue, K. Adsorption behavior of heavy metals onto chemically modified sugarcane bagasse. *Bioresour. Technol.* **2010**, *101*, 2067–2069. [[CrossRef](#)]
37. Sun, N.; Wen, X.; Yan, C. Adsorption of mercury ions from wastewater aqueous solution by amide functionalized cellulose from sugarcane bagasse. *Int. J. Biol. Macromol.* **2018**, *108*, 1199–1206. [[CrossRef](#)]

38. Gómez-Pastora, J.; Bringas, E.; Ortiz, I. Recent progress and future challenges on the use of high performance magnetic nano-adsorbents in environmental applications. *Chem. Eng. J.* **2014**, *256*, 187–204. [[CrossRef](#)]
39. Zhang, X.; Li, Y.; Hou, Y. Preparation of magnetic polyethylenimine lignin and its adsorption of Pb(II). *Int. J. Biol. Macromol.* **2019**, *141*, 1102–1110. [[CrossRef](#)]
40. Ji, J.; Chen, G.; Zhao, J. Preparation and characterization of amino/thiol bifunctionalized magnetic nanoadsorbent and its application in rapid removal of Pb (II) from aqueous system. *J. Hazard. Mater.* **2019**, *368*, 255–263. [[CrossRef](#)]
41. Guo, S.; Jiao, P.; Dan, Z.; Duan, N.; Zhang, J.; Chen, G.; Gao, W. Synthesis of magnetic bioadsorbent for adsorption of Zn(II), Cd(II) and Pb(II) ions from aqueous solution. *Chem. Eng. Res. Des.* **2017**, *126*, 217–231. [[CrossRef](#)]
42. Wang, Y.; Zhao, L.; Peng, H.; Wu, J.; Liu, Z.; Guo, X. Removal of Anionic Dyes from Aqueous Solutions by Cellulose-Based Adsorbents: Equilibrium, Kinetics, and Thermodynamics. *J. Chem. Eng. Data* **2016**, *61*, 3266–3276. [[CrossRef](#)]
43. Abdel-Aziz, H.M. Effective removal of chemical oxygen demand and phosphates from aqueous medium using entrapped activated carbon in alginate. *MOJ Biol. Med.* **2018**, *3*, 227–236. [[CrossRef](#)]
44. Pan, Y.; Zhu, Y.; Xu, Z.; Lu, R.; Zhang, Z.; Liang, M.; Liu, H. Adsorption Removal of COD from Wastewater by the Activated Carbons Prepared from Sugarcane Bagasse. In Proceedings of the 5th International Conference on Bioinformatics and Biomedical Engineering (iCBBE 2011), Wuhan, China, 10–12 May 2011; pp. 1–4. [[CrossRef](#)]
45. Sivashankar, R.; Sathya, A.; Sivasubramanian, V. Synthesis of magnetic biocomposite for efficient adsorption of azo dye from aqueous solution. *Ecotoxicol. Environ. Saf.* **2015**, *121*, 149–153. [[CrossRef](#)] [[PubMed](#)]
46. Alsuhybani, M.; Alshahrani, A.; Algamdi, M.; Al-Kahtani, A.A.; Alqadami, A.A. Highly efficient removal of Pb(II) from aqueous systems using a new nanocomposite: Adsorption, isotherm, kinetic and mechanism studies. *J. Mol. Liq.* **2020**, *301*, 112393. [[CrossRef](#)]
47. Tan, Y.; Wang, K.; Yan, Q.; Zhang, S.; Li, J.; Ji, Y. Synthesis of Amino-Functionalized Waste Wood Flour Adsorbent for High-Capacity Pb(II) Adsorption. *ACS Omega* **2019**, *4*, 10475–10484. [[CrossRef](#)] [[PubMed](#)]
48. Jafarnejad, M.; Asli, M.D.; Taromi, F.A.; Manoochehri, M. Synthesis of multi-functionalized Fe₃O₄-NH₂-SH nanofiber based on chitosan for single and simultaneous adsorption of Pb(II) and Ni(II) from aqueous system. *Int. J. Biol. Macromol.* **2020**, *148*, 201–217. [[CrossRef](#)]